Hypothesis article

A conserved arginine with non-conserved function is a key determinant of agonist selectivity in α7 nicotinic acetylcholine receptors

Teresa Minguez-Viñas[a], Beatriz E. Nielsen[b], Deborah K. Shoemark[c], Cecilia Gotti[d], Richard B. Sessions[c], Adrian J. Mulholland[e], Cecilia Bouzat[b], Susan Wonnacott[f], Timothy Gallagher[e], Isabel Bermudez[a][1], A Sofia Oliveira[c][e][2]

[a]Department of Biological and Medical Sciences, Oxford Brookes University, Oxford OX3 0BP (United Kingdom); [b]Instituto de Investigaciones Bioquímicas de Bahía Blanca, Departamento de Biología, Bioquímica y Farmacia, Universidad Nacional del Sur-Consejo Nacional de Investigaciones Científicas y Técnicas (CONICET), Bahía Blanca 8000 (Argentina); [c]School of Biochemistry, University of Bristol, Bristol BS8 1DT (United Kingdom); [d]CNR, Institute of Neuroscience, Biometra Department, University of Milan, I-20129 Milan (Italy); [e]School of Chemistry, University of Bristol, Bristol BS8 1TS (United Kingdom); [f]Department of Biology and Biochemistry, University of Bath, Bath BA2 7AY (United Kingdom).

Short Title: A β3-strand arginine is a subtype selectivity element in nAChR

Corresponding authors:

	* Isabel Bermudez	* A Sofia Oliveira
Email:	ibermudez@brookes.ac.uk	sofia.oliveira@bristol.ac

Keywords: Nicotinic acetylcholine receptors, agonist selectivity, cytisine, C(10) cytisine derivatives.

ABSTRACT

BACKGROUND AND PURPOSE:

The α7 and α4β2* (* denotes possibly assembly with another subunit) nicotinic acetylcholine receptors (nAChR) are the most abundant nAChR in the mammalian brain. These subtypes are also the most commonly targeted nAChR in drug discovery programs for brain disorders. However, the development of subtype specific agonists remains challenging, mainly due to the high degree of sequence homology coupled to the conservation of function in the nAChR family. Here, we determined the structural underpinning of the selectivity of 10-methylcytisine, a compound with high-affinity for α4β2 nAChR but negligible selectivity for the α7 subtype.

EXPERIMENTAL APPROACH:

The structural underpinning of the receptor selectivity of 10-methylcytisine was investigated using molecular dynamics simulations combined with mutagenesis and whole-cell and single-channel current recordings.

KEY RESULTS:

We identify a conserved arginine residue in the β3-strand that exhibits a non-conserved salt-bridge in the nAChR family. In α4β2 nAChR, the arginine forms an inter-subunit salt-bridge with an aspartate residue in loop B that is necessary for functional expression, whereas in the α7 subtype, this residue is not stabilised by electrostatic interactions, making its side chain highly mobile. This produces steric clashes with agonists and affects the dynamics of residues involved in agonist binding or the coupling network.

CONCLUSIONS AND IMPLICATIONS:

We conclude that the high mobility of the arginine residue in the α7 nAChR subtype affects agonist function by influencing agonist binding and the pathway communicating agonist binding to the ion channel. The findings have implications for rational design of subtype-selective cholinergic agents.

ABBREVIATIONS

Bungarotoxin, Bgtx; extracellular domain, ECD; nicotinic acetylcholine receptor, nAChR; cytisine, Cyt; 10-methylcytisine, MeCyt; principal component analysis, PCA; root mean square deviation, RMSD; root mean square fluctuation, RMSF.

1 INTRODUCTION

Nicotinic acetylcholine receptors (nAChR) are a major branch of the Cys loop neurotransmitter gated ion channel family, which also includes the $GABA_A$, glycine and $5\text{-}HT_3$ receptors (Corringer et al., 2000). The most prevalent nAChR in the mammalian brain are the $\alpha4\beta2$* (* denotes possibly assembly with another subunit) and α7 subtypes (Gotti et al., 2009). These subtypes are the most commonly targeted nAChR in drug discovery programs for neurological and neuropsychiatric disorders (Dineley et al., 2015). Additionally, $\alpha4\beta2$* nAChR play a central role in mediating the rewarding and reinforcing actions of nicotine (Maskos et al., 2005). Partial agonists of $\alpha7$ and $\alpha4\beta2$* nAChR are considered as a valid strategy to modulate the function of these subtypes in brain disorders and for aiding smoking cessation (Hogg and Bertrand, 2007; Coe et al., 2009). However, the development of specific $\alpha7$ or $\alpha4\beta2$ agonists remains challenging due to the structural similarity between nAChR (Corringer et al., 2000) (Figure S1A), and currently only the smoking cessation drugs varenicline (Champix®/Chantix®) and cytisine (Tabex®) are available clinically. However, despite the proven efficacy of varenicline (Hajek et al., 2013b) and cytisine (Hajek et al., 2013a) off-target effects continue to be problematic (Tonstad et al., 2010; Hajek et al., 2013b, 2013a). This is likely due to the ability of varenicline and cytisine to activate most nAChR subtypes, including the $\alpha7$ nAChR, at which they display full agonism, albeit with much-reduced binding and functional affinity than at $\alpha4\beta2$* nAChR, their intended target (Rego-Campello et al., 2018). Consequently, there is interest in identifying structural elements associated with agonist specificity that differ between the $\alpha4\beta2$ and $\alpha7$ nAChR.

Our work in this area has focused on developing cytisine analogues functionalised at position C(10) of the pyridone moiety (Figure 1A). These C(10) substituents are predicted to occupy a region in the agonist pocket between the complementary subunit and loop C of the principal subunit, enabling interactions with residues in both regions (Figure S1B) (Rego-Campello et al., 2018). Although we have found that the C(10) cytisine variants share the same core-binding interactions as cytisine in the $\alpha7$ and $\alpha4\beta2$ nAChR (Figure S1B), these compounds display negligible affinity for the $\alpha7$ subtype, while retaining selectivity for $\alpha4\beta2$ nAChR (Rego-Campello et al., 2018). A recent study using unnatural amino acid chain substitutions to probe the binding interactions of cytisine and its C(10) variants in the $\alpha4\beta2$ nAChR, showed that these substitutions only have a modest effect on interactions with residues in loop C and E, depending on the substituent's steric bulk or electronic effects (Blom et al., 2019); however, the conservation of these residues in $\alpha7$ nAChRs fails to explain the differential selectivity of the C(10) variants of cytisine.

To identify the structural elements underpinning the receptor selectivity of C(10) substituted cytisine variants, we have compared the dynamical behaviour of $\alpha7$ and $\alpha4\beta2$ nAChR bound to ACh, (-)cytisine or its C(10)-methyl variant, 10-methylcytisine (Figure 1A). Here, we identify a conserved arginine residue in

the β3-strand that in α7 nAChR not only orchestrates the suppression of agonism for 10-methylcytisine but also modulates agonist binding and channel function. In the α4β2 subtype, the analogous arginine residue mainly affects receptor expression. Our results have implications for the rational design of subtype-specific nAChR ligands.

2 METHODS

2.1 Materials

Varenicline and (-)cytisine were purchased from Tocris, UK. (-)-10-methylcytisine was synthesized at the Department of Chemistry, Bristol University (Rego-Campello et al., 2018). (±)-[^{3}H]Epibatidine (specific activity of 56-60 Ci/mmo) and [^{125}I]Bungarotoxin ([^{125}]Bgtx) (specific activity 200-213 Ci/mmol) were purchased from PerkinElmer, Boston MA. (±)Epibatidine, unlabeled bungarotoxin and collagenase Type 1A was from Sigma-Aldrich, UK.

2.2 Animals

All animal care and experimental procedures followed the guideline from the UK Home Office at the Biomedical Services, Oxford University. Adult female *Xenopus laevis* were purchased from *Xenopus* 1 (MI, USA) or Nasco (WI, USA). *Xenopus* toads were housed in a climate-controlled, light-regulated room. 50 toads were used. Toads were anaesthetised by immersion in 0.5% tricaine until no-responsive to toe pinch. Toads were then decapitated and ovarian lobes were harvested and defolliculated by incubation in 2 mg/ml collagenase Type IA. Oocytes were maintained until use at 18 $^{\circ}$C in a solution (OR2) containing 82 mM NaCl, 2 mM KCl, 2 mM $CaCl_2$, 5 mM HEPES; pH 7.6, supplemented with 20mg/ml of neomycin, 100 IU/ml penicillin and 100mg/ml streptomycin.

2.3 Single point mutations

Mutations were introduced in the α7, α4 or β2 nAChR subunits using the Stratagene QuikChange Site-Directed Mutagenesis Kit (Agilent, UK). The presence of the mutation and the absence of unwanted mutations were confirmed by sequencing the entire cDNA insert (Eurofins, UK). Note that we present the numbering of the residues according to the full length of the following UniProt sequence codes for human α4, β2 and α7 subunits, respectively: P43681 (α4 subunit), P17787 (β2 subunit) and P36544 (α7 subunit). To obtain the position in the mature form, subtract 28 from the number for α4, 25 for β2 and 22 from the α7 subunit.

2.4 *Xenopus* oocytes: expression of nAChR and two-electrode voltage clamp recordings

Electrophysiological experiments were carried out with wild type or mutant human α7 and α4β2 nAChRs expressed in *Xenopus laevis* oocytes. Oocytes were harvested from mature *Xenopus laevis* females and were prepared, injected with α7 or α4 and β2 cDNAs, and recorded using standard procedures, as described previously (Moroni et al., 2008; Rego-Campello et al., 2018). We expressed the two stoichiometries of the α4β2 nAChR. For the stoichiometry $(\alpha4)_3(\beta2)_2$, a mixture of 10 α4: 1 β2 cDNAs was injected into the nucleus of oocytes, whereas for the $(\alpha4)_2(\beta2)_3$ subtype the cDNA ratio injected was 1 α4:

10 β2. α7 cDNA was co-injected with chaperone NACHO at a ratio of 1 α7: 0.01 NACHO. Receptor expression was examined at least two days later, as previously described (Rego-Campello et al., 2018).

Oocytes were impaled with two electrodes filled with 3 M KCl, and their membrane potential was maintained at -60 mV throughout the experiment. All recordings were performed at 18°C, and cells were perfused with OR2 solution at pH 7.4. Currents were recorded using an automated platform equipped with standard two electrode voltage-clamp configuration (HiClamp; Multi Channel Systems, Reutlignen, Germany). This system differs from standard electrophysiology and other automated platforms because, instead of applying the compound in the perfusion, the oocyte is moved into a well from a 96-well microtiter plate containing 230 μl of the desired solution. Data were filtered at 10 Hz, captured at 100 Hz and analysed using proprietary data acquisition and analysis software running under Matlab (Mathworks Inc., Natick, MA) or Excel (Microsoft, Redmond, WA) combined with GraphPad Version 5 software (CA, USA). ACh, cytisine or 10-methylcytisine were prepared as concentrated stock solutions in water and then diluted in the recording medium to obtain the desired test concentrations. Agonist responses were determined using a protocol of 8-9 concentrations with a reference response (1 mM ACh, a maximal ACh concentration in all three wild type receptors tested) before and after compound testing. The agonists were applied for 10 s and the washing period between applications was 5 min.

Concentration-activation curves were fitted according to the Hill equation: $y = Imax/[1 (EC_{50}/[agonist])nH]$, where y is the normalised current amplitude, Imax is the maximal response (I_{max}/I_{AChMax}), EC_{50} is the agonist concentration at half-maximal efficacy, [agonist] is the agonist concentration, and nH the Hill coefficient. Curve fitting was carried out using the least squares method in MATLAB or using GraphPad software version 5. All agonist responses were normalised to the maximal concentration of ACh (1 mM). The fit was rejected if the estimated error in any fit parameter was greater than 60% of the fit value, and all parameter estimates for that fit were discarded. For compounds that elicited less than 10% of the maximal ACh response, the EC_{50} was not determined and the relative efficacy was established by using the equation: maximal response to test compound/maximal ACh response. Given the very low efficacy of cytisine at the α4β2 nAChR, this compound is able to competitively inhibit the ACh responses of nAChRs, which can be used to obtain a measure of the ability of this compound to bind the receptors. Therefore, we determined the concentration-response curve for the inhibition of current responses elicited by EC_{80} ACh concentrations [30 μM for $(\alpha4)_2(\beta2)_3$ or 300 μM for $(\alpha4)_3(\beta2)_2$] (see Table S2). The peak of the current responses was normalised to the appropriate control EC_{80} ACh concentration. The data were fit non-linearly to the Hill equation as described above. Data points for all concentration response plots represent the mean ± standard error of the mean (SEM) of 8-10 experiments carried out in at least five different batches of oocytes donors. The estimated EC_{50} or IC_{50} values are shown as mean ± 95% CI. The values for I_{max}/I_{AChMax} are shown as mean ± SEM.

2.5 Functional coupling of R101 to reporter mutation L9'T

The double-mutant cycle analysis was used to determine the coupling between α7 residue R101 and the reporter mutation L9'Tbinding site residues and gating, as previously used by Gleistman et al. (2009) to assess the functional coupling of agonist binding residues and gating. Residue L9' is located in the M2 and the L9'T is with a well-characterised reporter mutation known to impact gating in nAChR family (Revah et al., 1991). Functional coupling (Ω) between R101 and gating was estimated using the equation $\Omega = EC_{50}(AB) * EC_{50}(A'B')/EC_{50}(A'B) * EC_{50}(AB')$, where (AB) is α7 wild type, (A'B) is α7R101A, (AB') is α7L9'T and (A'B') is α7R101A/L9'T. If the two residues are functionally coupled, the double mutant α7R101A,L9'T should yield EC_{50} values that are greater than the product of the single mutant EC_{50} values, producing functional coupling (Ω); a value of Ω >2 is considered as meaningful coupling (Gleitsman et al., 2009). The macroscopic EC_{50} values were estimated by fitting ACh concentration response curve data to the Hill equation.

2.6 Single-channel recordings from mammalian cells

Single-channel currents were recorded from BOSC 23 cells co-transfected with α7 subunit (wild type or mutant) cDNA and the chaperone Ric-3 cDNA (1:4) by calcium phosphate precipitation. GFP cDNA (5 % of total cDNA amount) was incorporated during the transfection to allow identification of transfected cells. All transfections were carried out for about 8-12 hours in DMEM medium supplemented with 10% FBS, as previously described (Bouzat et al., 2008; Nielsen et al., 2018). Recordings were obtained in the cell-attached patch-clamp configuration at -70 mV. The bath and pipette solutions contained 142 mM KCl, 5.4 mM NaCl, 1.8 mM $CaCl_2$, 1.7 mM $MgCl_2$ and 10 mM HEPES (pH 7.4). We evaluated the effect of ACh and cytisine on wild type or mutant α7 receptors at their EC_{50} concentrations, which were determined from macroscopic concentration-response curves obtained from the two-electrode voltage clamp recordings carried out on oocytes described above (EC_{50} for ACh: 100 μM for α7 and α7G174D; EC_{50} for cytisine: 25 μM for α7 and 10 μM for α7G174D). The agonists were present in the pipette solution and typical recordings lasted 5-10 minutes. We did not test 10-methylcytisine due to its very low activity at the α7 nAChR (see Table 1). Single-channel currents were digitised at 5-10 μs intervals, low-pass filtered at a cut-off frequency of 10 kHz using an Axopatch 200B patch-clamp amplifier (Molecular Devices, CA, USA) and analysed using the program TAC (Bruxton Corporation, Seattle, WA, USA) with the Gaussian digital filter at 9 kHz (final cut-off frequency 6.7 kHz). Events were detected by the half-amplitude threshold criterion (Bouzat et al., 2008). To determine channel amplitude, events were tracked regardless of current amplitude and amplitude histograms were then constructed only for events longer than 0.3 ms to allow full resolution of α7 amplitude (Bouzat et al., 2008; Nielsen et al., 2018). Open-time histograms were fitted by the sum of exponential functions by maximum likelihood using the program TACFit (Bruxton Corporation, Seattle, WA, USA). Bursts of channel openings were identified as a series of closely separated openings preceded and followed by closings longer than a critical duration (Bouzat et al., 2008; Nielsen et al., 2018). Critical durations were defined by the intersection between the first and second briefest

components in the closed-time histogram for bursts of α7 or α7G174D (~200-400 μs), and the intersection between the second and third closed components for bursts of α7R101A (~2-5 ms). The longest duration closed components were not analysed because of their intrinsic variability as it depends on the expression level of α7 in each cell. Each patch corresponds to a different cell (n indicates the number of independent experiments). For each condition (distinct receptors or agonists), recordings were performed from three or more different cell transfections in different days (N indicates the number of cell transfections). Estimated parameters represent the mean ± standard deviation (SD).

2.7 Radioligand binding studies

[^{3}H]Epibatidine were carried out on membrane homogenates prepared from HEK 293 cells transfected with α4 and β2 cDNAs, as previously reported (Rego-Campello et al., 2018). For saturation experiments, the membrane homogenate aliquots were incubated overnight at 4 °C with 0.01-2.5 nM concentrations of (±)-[^{3}H]epibatidine. Nonspecific binding was determined in parallel by adding to the incubation solutions 100 nM unlabelled epibatidine. At the end of the incubation, the samples were filtered on a GFC filter soaked in 0.5% polyethylenimine and washed with 15 mL ice-cold PBS and the filters were counted in a β counter. For [^{125}I]Bungarotoxin ([^{125}]Bgtx) saturation binding studies were carried out on membrane homogenate prepared from SH-SY5Y cells transfected with human α7 cDNA, as described previously (Rego-Campello et al., 2018). Aliquots of the membrane homogenates were incubated overnight with 0.1-10.0 nM concentrations of [^{125}I]Bgtx at room temperature. Nonspecific binding was determined in parallel by including in the assay mixture 1 μM unlabeled Bgtx. After incubation, the samples were filtered as described for [^{3}H]epibatidine binding. For competition studies, the inhibition of [^{3}H]epibatidine and [^{125}I]Bgtx binding was measured by incubating the membranes transfected with the appropriate subtype with increasing concentrations of cytisine or 10-methylcytisine five minutes followed by overnight incubation at 4 °C, with [^{3}H]epibatidine 0.1 nM or at room temperature with [^{125}I]Bgtx 2-3 nM in the case of the α7 subtype. At the end of the incubation time, the samples were processed as described for the saturation studies. [^{125}I]Bgtx binding by measured by direct counting in an α counter.

Saturation binding data were evaluated by one-site competitive binding curve-fitting procedures using GraphPad Prism version 5 (GraphPad Software, CA, USA). In the saturation binding assay, the maximum specific binding (Bmax) and the equilibrium binding constant (Kd) values were calculated using one site–specific binding with Hill slope – model. K_i values were obtained by fitting three independent competition binding experiments, each performed in duplicate for each compound on each subtype. Inhibition constants (Ki) were estimated by reference to the Kd of the radioligand, according to the Cheng-Prusoff equation. All assays were carried out in triplicates and the data shown represent the mean ± 95% CI of three independent experiments (three different transfected cell batches).

2.8 Statistical analysis of functional data

Data and statistical analysis for all functional assays were blinded. The data and statistical analysis comply with the recommendations on experimental design and analysis in pharmacology (Curtis et al., 2015). LogEC_{50} values for agonist or inhibition concentration responses, changes in onset of current decay were analysed using one-way ANOVA, followed by a post hoc Dunnett's test and/or a posthoc Bonferroni multiple comparison test to determine the level of significance between wild type and mutant receptors. For single-channel data, two-tailed Student's *t*-tests with SigmaPlot 12.0 (Systat Software, Inc.) determined levels of statistical difference. For all the functional data shown here, differences between wild type and tests were considered statistical different if $p < 0.05$.

2.9 Molecular Dynamics Simulations

Molecular dynamics (MD) simulations of the extracellular domain (ECD) of wild type and mutant human α4β2 or α7 nAChR subtypes were performed to identify the molecular factors that control the selectivity of the C(10) variants of cytisine. The ECD of the human α4β2 nAChR (PDB code: 5KXI) (Morales-Perez et al., 2016) was used as the starting point for all α4β2 systems whereas the homology model of the human α7 nAChR taken from our previous work (Rego-Campello et al., 2018) was the starting point for all α7 simulations. All systems were simulated with ACh, cytisine or 10-methylcytisine bound to two nonconsecutive binding pockets. It has been shown experimentally that the binding of agonists to two nonconsecutive binding pockets enables proper activation of homomeric Cys loop receptors (Bouzat et al., 2009). ACh was placed in the binding pockets in a position analogous to the one observed in the crystal structure of the AChBP from *Aplysia Californica* (PDB code: 2XZ5) (Brams et al., 2011). The binding modes of cytisine and 10-methylcytisine were the same as the ones previously described in (Rego-Campello et al., 2018). The protonation state of the protonatable groups was determined using a combination of Poisson-Boltzmann, and Metropolis Monte Carlo calculations, as previously described (Oliveira et al., 2019). Based on these calculations, all protonatable residues were found to be in their standard state at a physiological pH. The three agonists (ACh, cytisine and 10-methylcytisine) were considered to be positively charged. All MD simulations were performed using Gromacs (version 5.1.4) on the University of Bristol's High-Performance Computer, BlueCrystal (Phase 4) (Abraham et al., 2015). The Amber ff99SB-ILDN (Lindorff- Larsen et al., 2010) force-field was used to describe the protein. The parameters for cytisine and 10-methylcytisine were taken from our previously published work (Rego-Campello et al., 2018). Acpype (Sousa da Silva and Vranken, 2012) was used to generate Amber-GAFF parameters for ACh. All systems were solvated using TIP3P waters (Jorgensen et al., 1983). The simulations were performed at the constant temperature of 310 K, and the velocity-rescaling thermostat was used, with separate couplings for the solutes (protein and agonists) and solvent, using a relaxation time constant of 0.1 ps. A Berendsen barostat was used to keep the pressure at 1 bar, with a coupling constant of 1 ps. A time step of 2 fs was used for integrating the equations of motion. Non-bonded long-range electrostatic interactions were calculated using the smooth particle mesh Ewald method beyond a

12 Å cutoff. The same 12 Å cutoff was used for the van der Waals interactions with long-range dispersion corrections for the energy and pressure. The neighbour lists were updated every 20 steps. All systems were energy minimised, equilibrated and simulated according to the protocol as previously described (Rego-Campello et al., 2018). Five unrestrained MD simulations were performed for each of the following protein-agonist complexes: α4β2, α4β2R106A, α7, α7R101A and α7G174D, each bound to ACh, cytisine or 10-methylcytisine**.** All systems were energy minimised, equilibrated and simulated according to the protocol described in (Rego-Campello et al., 2018). Five unrestrained simulations, each 100-ns long, were performed for each protein-agonist complex, in a total of 7.5 μs of simulation.

2.10 Analysis of the MD simulations

All the analyses were performed using Gromacs (Abraham et al., 2015) and in-house tools. Principal component analysis (PCA) was used to examine the sampling of the replicates, as previously described (Oliveira et al., 2019), and identify the differences between wild type and mutant receptors (data available upon request). Each PCA trajectory contained one conformation per nanosecond per replicate (totaling 5001 frames). The two principal components (PC1 and PC2) were used to assess the equilibration/relaxation of the simulations, and all systems were considered equilibrated after 50 ns. The different replicates sampled different regions of conformational, thus improving the overall sampling for each system.

The structural stability of the agonist-bound and unbound receptor complexes was examined by monitoring two system properties, namely the C_α root mean square deviation (RMSD) from the starting structure and the secondary structure content, as previously described in (Oliveira et al., 2019). Both systems remained stable over the simulation time, and the average C_α RMSD profiles showed a plateau after 50 ns (data shown on request). The stability of the systems was further demonstrated by the analysis of the secondary structure content of the receptor using the hydrogen bond estimation algorithm DSSP (Kabsch and Sander, 1983) with only a small secondary structure loss (< 2%).

2.11 Nomenclature of targets and ligands

Key protein targets and ligands in this article are hyperlinked to corresponding entries in **http://www.guidetopharmacology.org**, the common portal for data from the IUPHAR/BPS Guide to PHARMACOLOGY (Harding et al., 2018), and are permanently archived in the Concise Guide to PHARMACOLOGY 2017/18 (Alexander et al., 2017).

3 RESULTS

3.1 An arginine residue in β3-strand affects agonist selectivity

Recently, we suggested that differences in several residues in the binding pocket of the α7 and α4β2 nAChR may account for the selectivity of 10-methylcytisine (Rego-Campello et al., 2018); however, functional assays of relevant mutant variants failed to demonstrate the involvement of these residues on agonist effects (Table S1), thus leaving the question of the selectivity of 10-methylcytisine unanswered. Here, we explored the differences between the subtype binding sites by performing MD simulations of α4β2 and α7 nAChR ECD complexes with ACh, cytisine or 10-methylcytisine. Note that 10-methylcytisine represents a relatively modest modification of cytisine with the addition of a sterically undemanding methyl moiety, lacking any polar component capable of interacting with other residues.

MD simulations revealed distinct patterns of dynamical behaviour of the agonists bound to α7 or α4β2 nAChR. In the α4β2 complexes, ACh exhibited high mobility, adopting many different binding modes while inside the agonist binding pocket (Figure 1B). As expected from their more rigid structures and additional cation-π interaction with loop C compared to ACh (Blom et al., 2019), cytisine and 10-methylcytisine showed less mobility, generally remaining in the same orientation throughout the simulation. In contrast, in the α7 complexes, all agonists exhibited greater positional and conformational variability, regardless of the steric bulk and rigidity of the ligands (Figure 1B).

The MD simulations led us to identified an arginine residue located in β3-strand of the α7 (R101) and β2 (R106) subunits as key in distinguishing α7 from α4β2 (Figures 2A, 2B; Figure S2). This residue is conserved in the nAChR family (Figure S3) and has been reported to affect agonist potency in bovine α7 nAChR (Criado et al., 2011). In the α7 complex, the side chain of R101 was highly mobile (Figure 2A; Figure S2; Movie 1) as it lacked a nearby negatively charged residue to form stable electrostatic interactions with (Figure 2A). While sampling the space, the side chain of R101 oriented downward towards the inside of the binding pocket establishing transient interactions with loop C residues, notably with E215 (Figure 3A). The side chain of R101 was even able to approach the C(10) position of the cytisine scaffold, which in the 10-methylcytisine-α7 complex resulted in the loss of interactions between 10-methylcytisine and loop C residues Y210 (TyrC1) and Y217 (TyrC2) of the agonist binding pocket (Figure 2C; Movie 1). (See Figure S1A for a model of the agonist binding pocket in nAChRs).

In contrast, in α4β2, β2R106 was less mobile as it established a salt-bridge with an aspartate residue (α4D185) from loop B (Figures 2B, 3B; Figure S2) and only transiently with a glutamate residue in loop C (α4E228) that is equivalent to α7E215 (Figure 3C). The aspartate residue in loop B is not conserved in the α7 subtype (Figure S3). While the salt-bridge between α4D185 and β2R106 was stable during the

simulation (Figure 3B), the interaction with α4E228 was less frequent than that of its counterpart in the α7 complex (R101-E215) (Figures 3A, C). Preliminary [^{3}H]epibatidine binding assays on clonal cells expressing α4β2 nAChRs showed that D185G reduced maximal binding (Bmax) without changes in binding affinity (K_D) (Table S2). In line with these findings, two-electrode voltage recordings from *Xenopus* oocytes expressing α4D185Gβ2 or α4β2R106A receptors revealed reduced functional expression without changes in agonist potency (Table S2).

3.2 Arginine in β3-strand influences agonist binding and function in α7 nAChR

Given the role of TyrC1 and TyrC2 in agonist binding in α7 (Corringer et al., 1995; Puskar et al., 2011), we speculated that the loss of the interactions with these tyrosine residues could explain the negligible affinity of 10-methylcytisine for the α7 subtype. Our aim was to mimic the α4β2 salt-bridge between β2R106 and α4D185 in α7, by mutating α7G174 to aspartate (α7G174D) to allow a salt-bridge to form with R101. MD simulations of α7G174D showed that R101 forms an inter-subunit salt-bridge with G174D (Figure 4A). This salt-bridge not only influenced the correlated motions (Figure S4) and dynamics (Figure S5) between the two subunits but also reduced the frequency of the interaction between R101 with E215 of loop C (Figure 4B). G174D also induced ligand-dependent changes in the distribution of the distances between the ligands and the conserved aromatic residues of the agonist binding pocket, particularly with α7Y115 (TyrA) and α7W77 (TrpD) (Figure 4C, D; Figure S6). This finding is significant because TyrA and TrpD are pivotal for the binding mode of agonists in the α7 subtype (Horenstein et al., 2007; Williams et al., 2009; Puskar et al., 2011; Arnam et al., 2013).

To assess the functional impact of G174D on agonist effects, we obtained activation concentration-response curves for ACh and the cytisine compounds from α7G174D receptors expressed in *Xenopus* oocytes. As shown in Figure 5A and Table 1, G174D increased the potency of cytisine and 10-methylcytisine but had no effects on ACh function (Table 1). The maximal responses of cytisine remained wild type but that of 10-methylcytisine almost doubled (Table 1). Preliminary saturation [^{125}I]αBgtx binding assays showed no differences in the apparent K_D values for α7 and α7G174D receptors (α7 K_D 0.32 nM; α7G174D K_D 0.33 nM) or the maximal binding capacity (B_{max}) (α7, 463 ± 12.7 fmol/mg prot; α7G174D, 430 ± 10.6 fmol/mg prot.). However, competition assays showed that G174D enhances the ability of cytisine and 10-methylcytisine to displace [^{125}I]αBgtx binding (cytisine K_i: α7, 855 (528-1386) nM; α7G174D, 169 (108-265) nM. 10-methylcytisine K_i: α7, 5371(2650-10880) nM; α7G174D, 458 (275-760). Therefore, the G174D does not alter [^{125}I]αBgtx maximal binding but enhances the binding affinity and the functional potency of cytisine and 10-methylcytisine in α7.

To understand if the functional effects of G174D are due to the stabilization of R101 through salt-bridge interactions, we assessed the functional consequences of the distance between charged side chains in

position 174 and 101. For this, we examined the effects of the three agonists on α7G174D,R101K, α7G174E and α7G174E,R101K (Figure 5B). As expected from the distance dependency of salt-bridges, variations in the distance between residues in positions 174 and 101 influenced agonist potency (Figure 5B-C; Table 1). Reversal of charge, R101D or G174D-R101D, decreased functional expression to less than 5-10% of wild type levels (Table 1). Therefore, R101 through inter-subunit salt-bridge interactions increases agonist potency but reversal of charge at this position (R to D) is not tolerated.

3.3 G174D increases the duration of activation episodes in α7 nAChR

To decipher the effect of G174D on agonist action at the molecular level, we performed cell-attached patches in the presence of EC_{50} ACh or cytisine in the pipette solution. We did not test 10-methylcytisine due to its very low activity and potency at the α7 nAChR (Table 1) (Rego-Campello et al., 2018). For α7 nAChR, ACh or cytisine single-channel activity appeared as single brief pulses flanked by long-closed periods or occasionally as bursts of several openings in quick succession (Figure 6A), which correspond to activation episodes of a single receptor molecule (Bouzat et al., 2008; Nielsen et al., 2018). A wide range of channel amplitudes are detected because the brief open-channel lifetime does not allow full amplitude resolution (Bouzat et al., 2008). Amplitude histograms for events longer than 0.3 ms that were fully resolved yielded a mean value of ~10 pA (9.99 ± 0.41 pA for both agonists, in agreement with previously published data for ACh (Bouzat et al., 2008; Nielsen et al., 2018). Whilst there were no statistically significant differences in the mean open duration of α7 receptors activated by ACh or cytisine 1 (~0.28 ms), the burst duration in the presence of cytisine was significantly longer (~0.72 ms) than in the presence of ACh (~0.33 ms) (Figure 6B; Table 2). This finding is in line with the greater sensitivity of α7 receptors to activation by cytisine, compared to ACh. For α7G174D nAChR, the single-channel amplitude (10.01 ± 0.26 pA) and the mean open duration for ACh or cytisine were comparable to wild type (Figure 6B, Table 2). However, for both agonists, the mean burst durations increased by ~2 fold, compared to wild type (Figure 6B, Table 2). Therefore, G174D increases agonist potency by increasing burst duration. The increase in burst duration could be due to slower receptor desensitisation rates. Although the desensitisation rate of α7 receptors cannot be accurately determined from the decay rate of macroscopic currents, particularly in relatively slow temporal systems (Bouzat et al., 2008), a change in the desensitisation rate should translate to a change in the decay rate. We did not observe changes in the half-life of the onset of current decay in α7G174D (α7 0.250 ± 0.02 ms *vs* α7G174D 0.464 ± 0.1 s; n = 8) (Figure 6C). Additionally, we found no differences between the half-life of current decay of the fast and slow phase components (fast decay: α7 0.360 ± 0.1 s *vs* α7G174D 0.330 ± 0.1 s; slow decay: α7 1.8 ± 0.7 s *vs* α7G174D 1.1 ± 0.8 s; n = 8).

3.4 α7R101A affects agonist potency, burst duration and onset of current decay

Given the impact of R101 mobility on agonist potency, we speculated that alanine substitution of R101 should abolish the steric clash with bulkier agonists, leading to an increase in agonist potency. However, as shown in Figure 7A and Table 1, R101A decreased the potency of all agonists tested. The greatest decrease was observed for ACh and cytisine (~11 fold). For cytisine, R10A caused a ~4-fold increase in relative efficacy (Table 1). These findings raised the possibility that the steric clash effect of R101 is not the only factor by which this residue affects agonist action at α7 nAChR. A likely additional factor could be that due to the mobility of its side chain, R101defines the electrostatic landscape in the top part of the binding pocket (Figure S7). If charge is important, reversal of charge should impair function. Figure 7B shows that the R101D mutation decreased the maximal responses of ACh by ~95% and slowed the onset of the decay of the responses.

R101A had no effects on the single channel amplitude of ACh or cytisine currents compared to wild type (10.12 ± 0.26 pA and 9.99 ± 0.41 pA, respectively, n=8; N =5). Also, R101A had no effects on the mean open duration of the single currents activated by either agonist (Figure 7C; Table 2). In contrast, R101A increased the mean burst duration by ~3-to 4-fold, compared to wild type and, surprisingly, by 2-fold compared to G174D (Figure 7C; Table 2). Unlike G174D, the increase in burst duration produced by R101A does not translate into increased agonist potency (Table 1). However, we observed a decrease in the decay rate on the macroscopic ACh current responses of α7R101A receptors expressed in *Xenopus* oocytes (Figure 7B). The onset of current decay decreased by 4-fold compared to wild type (α7 0.25 ± 0.02 s *vs* α7R101A 1.02 ± 0.05 s; n = 8; N =5) (Figure 7B). The data fitted by two exponential components showed that the mutation increased the fast decay half-life (α7, 0.360 ± 0.1 s *vs* α7R101A, 1.01 ± 0.05 s; n = 8) but not the slow decay half-life (α7, 1.8 ± 0.7 s *vs* α7R101A, 1.1 ± 0.8 s; n = 8; N=5). Thus, decreased desensitisation rate may account for both the increase in cytisine efficacy and longer duration bursts, even with the reduced potency of both agonists, as bursts terminate by desensitisation of the receptor.

MD simulations of α7R101A complexes provided insights into the impact of R101A on the dynamics of the receptor. For all three agonists, analysis of the Root Mean Square Fluctuations (RMSF) profiles of the C*α* atoms between α7 and α7R101A showed differences in the binding site region and in the structural motifs involved in inter-domain communication. In the ACh-bound complexes, the largest differences are located in loops A, B and Cys loop (Figure 8; Figure S8). In complexes involving cytisine, the most noticeable differences are observed in loops A, B, E and F and loop Cys (Figure 8; Figure S8). In 10-methylcytisine complexes, the differences are in loops C, D, E and F and loop Cys (Figure 8; Figure S8).

Comparisons of the average structures of α7 and α7R101A highlighted differences in loops C and F mainly when in the presence of the bulkier ligands (Figure 9; Figure S9). The difference in the loop C region is likely due to the loss of the electrostatic interaction between R101 and E215 in loop C. This interaction is important for agonist function, as revealed by the reduced potency of all three ligands at α7E215A receptors (Table 1). To compensate for the loss of the E215-R101 interaction in α7R101, E215 (very) transiently formed a salt-bridge with K98 (located close to R101) (Figure S10). In the case of cytisine, the agonist most affected by mutations E215A or R101A (see Table 1), the (low) frequency of this new interaction affects the closing of loop C (Figure 9; Figure S9). Analysis of the distribution of distance between agonists and the conserved aromatic residues of the agonist pocket were similar for all three agonists, except for TyrA, which for cytisine varied between the α7 and α7R101A systems (Figure S11).

3.5 R101 couples to gating

The dynamic links between R101 and the Cys loop and loop F, which have been linked to the agonist-binding-gating coupling network in α7 nAChR (Oliveira et al., 2019), led us to examine whether R101 couples to gating. We tested this possibility using the double-mutant cycle analyses. Here, the R101A mutation was combined with a reporter mutation (L9'T) known to impact gating (Revah et al., 1991). If the two residues are functionally coupled, the double mutant α7R101A,L9'T should yield EC_{50} values that are greater than the product of the single mutant EC_{50} values, producing functional coupling (Ω); a value of Ω >2 is considered as meaningful coupling (Gleitsman et al., 2009). For R101A, the estimated Ω for coupling to L9'T was 2.4, indicating coupling between R101 and L9'T.

4 DISCUSSION

For the purpose of developing partial agonists for the α4β2 nAChR with improved selectivity, we generated a range of diverse and enantiomerically pure C(10) variants of cytisine, exampled by the 10-methyl analogue (Rego-Campello et al., 2018). These variants display increased affinity for α4β2 but, despite the more permissive nature of the agonist binding pocket α7 (Horenstein et al., 2007), they exhibit negligible affinity for the α7 nAChR (Rego-Campello et al., 2018). Here we identify a salt-bridge between an aspartate residue in loop B of the α4 subunit (α4D185) and a conserved arginine in β3-strand as key in distinguishing α4β2 from α7 nAChR. In α7 nAChR, the salt-bridge is not conserved as the aspartate is replaced by a glycine, conferring greater mobility to the arginine residue in this nAChR subtype. For cytisine and its 10-methyl variant, this mobility leads to steric clashes that manifest as competition for the space associated with the agonist binding site. For 10-methylcytisine, this weakens the interaction with TyrC1 and TyrC2 in loop C, which ultimately ablates the binding of this variant. When the mobility of R101 is reduced through a salt-bridge with G174D, agonists achieve optimal binding interactions, depending on the steric bulk and the binding mode of the agonist. These interactions likely increase the strength of agonist binding and/or enhance the efficacy for activation, allowing α7G174D to activate in episodes or bursts that are very infrequent in α7 nAChR.

Underlying the impact of R101 on agonist binding is the interaction of R101 with E215 in loop C. This interaction influences the dynamical behavior of loop C, which in α7R101A, and for cytisine only, impacts loop C capping. Although the role of loop C capping in shaping channel gating is still under debate (Purohit and Auerbach, 2013), its role in anchoring bound agonist to the binding site is well established (Auerbach, 2015). Therefore, in the context of the α7 nAChR, the R101-E215 interaction may influence agonist access to TyrC1 and TyrC2, which ultimately may define the strength of the anchoring of bound agonist to the agonist pocket, and therefore agonist potency.

Mutant cycle analysis indicated functional coupling between R101 and L9'T, a reporter mutation for gating (Revah et al., 1991). Given that R101 is located in the ECD, ~50 Å from L9'T in the ion channel, the coupling is essentially allosteric and could stem from the impact of R101 on the dynamics of residues implicated in gating through agonist binding and/or in the communication of agonist binding to the gating domain. Our MD simulations of α7R101A complexes suggested that R101 modulates the dynamical behavior of residues known to bind agonists in the α7 nAChR, such as Tyr A , TyrC1, TyrC2 and TrpD (Corringer et al., 1995; Fruchart-Gaillard et al., 2002; Horenstein et al., 2007; Williams et al., 2009; Puskar et al., 2011). Additionally, our studies also revealed R101-dependent changes in the dynamical behavior of the Cys loop and loop F. These loops have been linked to the coupling network in α7 nAChR (Oliveira et al., 2019). Although our findings do not reveal how R101 impacts the dynamics of these loops, the effects are clearly exerted through indirect interactions. Given the mobility of the charged side chain of

R101, these mechanisms may be related to the electrostatic environment created by R101. Previous studies have shown the role of the electrostatic field around the agonist site for steering the neurotransmitter into the binding site (Carpenter and Lightstone, 2016), the ligand association rate in the agonist site of the muscle nAChR (Meltzer et al., 2006) and capping of loop C in the α9α10 nAChR (Azam et al., 2015).

R101A slows down the onset of the decay, suggesting R101 plays a role in the onset of desensitisation of the α7 nAChR. This finding adds further insights on the structural mechanisms of desensitisation in the α7 nAChR. Although the kinetics of the decay of the macroscopic current responses in α7 nAChR does not reflect exactly the desensitisation of this receptor, it provides sufficient insight to enable us to draw some conclusions on how R101 may influence this process. The structural mechanisms of α7 nAChR desensitisation are not completely understood; however, TrpD has been reported to slow down the onset of desensitisation and recovery (Gay et al., 2008). Therefore, since R101 affects the dynamical behavior of TrpD, the impact of R101 on α7 nAChR desensitisation could stem from the TrpD-R101 link. Considering that TrpD is close to coupling elements (e.g., the β1-β2 linker) and that desensitisation may be initiated by the uncoupling of the coupling region (Revah et al., 1991; Zhang et al., 2011), movement of TrpD during agonist binding could trigger uncoupling. In this context, the effect of R101 on desensitisation of the α7 nAChR could be based on R101 being able to fine-tune the structural changes of TrpD that affect the uncoupling of the gating machinery.

In the α4β2 nAChR, R106 does not affect receptor function but is necessary for functional expression. This finding suggest a role in receptor assembly or trafficking to the membrane, as is the case for an equivalent arginine residue in the $GABA_A$ receptor (Hales et al., 2005). The salt-bridge between the arginine in β3-strand and the aspartate in loop B is highly conserved among heteromeric nAChRs (Figure S3). In the nAChR family, functional divergence seems to have been achieved through heteromeric receptors. In this context, and considering that salt-bridges bring stability to multimeric protein ensembles (Sokalingam et al., 2012), one can speculate that the salt-bridge between the β3-strand arginine and loop B aspartate emerged during the evolution of nAChR to aid the stabilisation of heteromeric receptor ensembles. Exceptionally, neither the α9 nor α10 nAChR, which form α9α10 nAChR, conserve such an interaction. This may be due to that neither of these subunits appears to have followed the same evolutionary trajectories as the other nAChR subunits: α9 and α10 subunits show great divergence in coding sequence and a highly restrictive ability to assemble with other nAChR subunits (Marcovich et al., 2020).

Conclusion and significance

We showed R101 in the β3-strand as a key agonist selectivity element in the α7 nAChR. The side chain of R101 is highly mobile, which not only affects agonist binding but also defines the electrostatic field on the top region of the agonist site, which appears to have a global influence on α7 nAChR function. A key feature in the role of R101 in receptor function and agonist selectivity is its association with loop C, which shapes agonist binding. R101 couples to gating and affects desensitisation, likely through its effects on TrpD dynamics. Integration of these insights into molecular design activity will help to develop ligands incorporating specific functional moieties that allow for interaction with R101 in β3-strand. This offers a potential strategy for increasing discrimination and affinity for the resulting receptor-ligand complex as a screen to identify more selective agents with enhanced therapeutic potential.

ACKNOWLEDGEMENTS

We thank EPSRC (EP/N024117/1) for financial support and Achieve Life Sciences for a generous gift of (-)-cytisine. All MD simulations were carried out using the computational facilities of the Advanced Computing Research Centre, University of Bristol (http://www.bris.ac.uk/acrc). A.J.M. also thank EPSRC for funding for CCP-BioSim, the UK Collaborative Computational Project on Biomolecular Simulation (ccpbiosim.ac.uk) under grant no. EP/ M022609/1. TM was funded by A Nigel Groome Brookes University studentship. Single channel work was supported by grants from Universidad Nacional del Sur (PGI 24/B227) to CB and from Agencia Nacional de Promoción Cientifica y Tecnológica (PICT-2015-0941 and PICT-2017-1170).

CONFLICT OF INTEREST

The authors declare no conflict of interest.

AUTHORS CONTRIBUTION

CB, CG, DKS, RBS, AJM, IB, ASO designed research. TM, BEN, CG, IB, ASO performed research and analysed data. IB, TG, ASO, SW, AJM, CB, BEN wrote paper. IB, CB provided supervision.

DECLARATION OF TRANSPARENCY AND SCIENTIFIC RIGOUR

This Declaration acknowledges that this paper adheres to the principles for transparent reporting and scientific rigour of preclinical research as stated in the *BJP* guidelines for **Design & Analysis** and as recommended by funding agencies, publishers, and other organisations engaged with supporting research.

REFERENCES

Abraham, M.J., Murtola, T., Schulz, R., Páll, S., Smith, J.C., Hess, B., et al. (2015). GROMACS: High performance molecular simulations through multi-level parallelism from laptops to supercomputers. SoftwareX *1–2*: 19–25.

Alexander, S.P., Kelly, E., Marrion, N.V., Peters, J.A., Faccenda, E., Harding, S.D., et al. (2017). THE CONCISE GUIDE TO PHARMACOLOGY 2017/18: Overview. British Journal of Pharmacology *174*: S1–S16.

Arnam, E.B.V., Blythe, E.E., Lester, H.A., and Dougherty, D.A. (2013). An Unusual Pattern of Ligand-Receptor Interactions for the α7 Nicotinic Acetylcholine Receptor, with Implications for the Binding of Varenicline. Mol Pharmacol *84*: 201–207.

Auerbach, A. (2015). Agonist activation of a nicotinic acetylcholine receptor. Neuropharmacology *96*: 150–156.

Azam, L., Papakyriakou, A., Zouridakis, M., Giastas, P., Tzartos, S.J., and McIntosh, J.M. (2015). Molecular Interaction of α-Conotoxin RgIA with the Rat α9α10 Nicotinic Acetylcholine Receptor. Mol Pharmacol *87*: 855–864.

Blom, A.E.M., Campello, H.R., Lester, H.A., Gallagher, T., and Dougherty, D.A. (2019). Probing Binding Interactions of Cytisine Derivatives to the α4β2 Nicotinic Acetylcholine Receptor. J. Am. Chem. Soc. *141*: 15840–15849.

Bouzat, C., Bartos, M., Corradi, J., and Sine, S.M. (2008). The Interface between Extracellular and Transmembrane Domains of Homomeric Cys-Loop Receptors Governs Open-Channel Lifetime and Rate of Desensitization. J. Neurosci. *28*: 7808–7819.

Bouzat, C.B., Rayes, D., Rosa, M.J.D., and Sine, S.M. (2009). Electrical Fingerprinting Reveals Agonist Binding Sites Required for Activation of Homo-pentameric Cys-loop Receptors. Biophysical Journal *96*: 167a.

Brams, M., Gay, E.A., Sáez, J.C., Guskov, A., Elk, R. van, Schors, R.C. van der, et al. (2011). Crystal Structures of a Cysteine-modified Mutant in Loop D of Acetylcholine-binding Protein. J. Biol. Chem. *286*: 4420–4428.

Carpenter, T.S., and Lightstone, F.C. (2016). An Electrostatic Funnel in the GABA-Binding Pathway. PLOS Computational Biology *12*: e1004831.

Coe, J.W., Rollema, H., and O'Neill, B.T. (2009). Chapter 4 Case History: Chantix™/Champix™ (Varenicline Tartrate), a Nicotinic Acetylcholine Receptor Partial Agonist as a Smoking Cessation Aid. In Annual Reports in Medicinal Chemistry, J.E. Macor, ed. (Academic Press), pp 71–101.

Corringer, P.-J., Galzi, J.-L., Eiselé, J.-L., Bertrand, S., Changeux, J.-P., and Bertrand, D. (1995). Identification of a New Component of the Agonist Binding Site of the Nicotinic 7 Homooligomeric Receptor. J. Biol. Chem. *270*: 11749–11752.

Corringer, P.-J., Novère, N.L., and Changeux, J.-P. (2000). Nicotinic Receptors at the Amino Acid Level. Annu. Rev. Pharmacol. Toxicol. *40*: 431–458.

Criado, M., Mulet, J., Gerber, S., Sala, S., and Sala, F. (2011). Mutants of β-strand β3 and the loop B in the interface between α7 subunits of a homomeric acetylcholine receptor show functional and pharmacological alterations. Journal of Neurochemistry *118*: 968–978.

Curtis, M.J., Bond, R.A., Spina, D., Ahluwalia, A., Alexander, S.P.A., Giembycz, M.A., et al. (2015). Experimental design and analysis and their reporting: new guidance for publication in BJP. British Journal of Pharmacology *172*: 3461–3471.

Dineley, K.T., Pandya, A.A., and Yakel, J.L. (2015). Nicotinic ACh receptors as therapeutic targets in CNS disorders. Trends in Pharmacological Sciences *36*: 96–108.

Fruchart-Gaillard, C., Gilquin, B., Antil-Delbeke, S., Novère, N.L., Tamiya, T., Corringer, P.-J., et al. (2002). Experimentally based model of a complex between a snake toxin and the α7 nicotinic receptor. PNAS *99*: 3216–3221.

Gay, E.A., Giniatullin, R., Skorinkin, A., and Yakel, J.L. (2008). Aromatic residues at position 55 of rat α7 nicotinic acetylcholine receptors are critical for maintaining rapid desensitization. The Journal of Physiology *586*: 1105–1115.

Gleitsman, K.R., Shanata, J.A.P., Frazier, S.J., Lester, H.A., and Dougherty, D.A. (2009). Long-Range Coupling in an Allosteric Receptor Revealed by Mutant Cycle Analysis. Biophysical Journal *96*: 3168–3178.

Gotti, C., Clementi, F., Fornari, A., Gaimarri, A., Guiducci, S., Manfredi, I., et al. (2009). Structural and functional diversity of native brain neuronal nicotinic receptors. Biochemical Pharmacology *78*: 703–711.

Hajek, P., McRobbie, H., and Myers, K. (2013a). Efficacy of cytisine in helping smokers quit: systematic review and meta-analysis. Thorax *68*: 1037–1042.

Hajek, P., Stead, L.F., West, R., Jarvis, M., Hartmann-Boyce, J., and Lancaster, T. (2013b). Relapse prevention interventions for smoking cessation. Cochrane Database of Systematic Reviews.

Hales, T.G., Tang, H., Bollan, K.A., Johnson, S.J., King, D.P., McDonald, N.A., et al. (2005). The epilepsy mutation, γ2(R43Q) disrupts a highly conserved inter-subunit contact site, perturbing the biogenesis of GABAA receptors. Molecular and Cellular Neuroscience *29*: 120–127.

Harding, S.D., Sharman, J.L., Faccenda, E., Southan, C., Pawson, A.J., Ireland, S., et al. (2018). The IUPHAR/BPS Guide to PHARMACOLOGY in 2018: updates and expansion to encompass the new guide to IMMUNOPHARMACOLOGY. Nucleic Acids Res *46*: D1091–D1106.

Hogg, R.C., and Bertrand, D. (2007). Partial agonists as therapeutic agents at neuronal nicotinic acetylcholine receptors. Biochemical Pharmacology *73*: 459–468.

Horenstein, N.A., McCormack, T.J., Stokes, C., Ren, K., and Papke, R.L. (2007). Reversal of Agonist Selectivity by Mutations of Conserved Amino Acids in the Binding Site of Nicotinic Acetylcholine Receptors. J. Biol. Chem. *282*: 5899–5909.

Jorgensen, W.L., Chandrasekhar, J., Madura, J.D., Impey, R.W., and Klein, M.L. (1983). Comparison of simple potential functions for simulating liquid water. J. Chem. Phys. *79*: 926–935.

Kabsch, W., and Sander, C. (1983). Dictionary of protein secondary structure: Pattern recognition of hydrogen-bonded and geometrical features. Biopolymers *22*: 2577–2637.

Lindorff-Larsen, K., Piana, S., Palmo, K., Maragakis, P., Klepeis, J.L., Dror, R.O., et al. (2010). Improved side-chain torsion potentials for the Amber ff99SB protein force field. Proteins: Structure, Function, and Bioinformatics *78*: 1950–1958.

Marcovich, I., Moglie, M.J., Carpaneto Freixas, A.E., Trigila, A.P., Franchini, L.F., Plazas, P.V., et al. (2020). Distinct Evolutionary Trajectories of Neuronal and Hair Cell Nicotinic Acetylcholine Receptors. Mol Biol Evol *37*: 1070–1089.

Maskos, U., Molles, B.E., Pons, S., Besson, M., Guiard, B.P., Guilloux, J.-P., et al. (2005). Nicotine reinforcement and cognition restored by targeted expression of nicotinic receptors. Nature *436*: 103–107.

Meltzer, R.H., Thompson, E., Soman, K.V., Song, X.-Z., Ebalunode, J.O., Wensel, T.G., et al. (2006). Electrostatic Steering at Acetylcholine Binding Sites. Biophysical Journal *91*: 1302–1314.

Morales-Perez, C.L., Noviello, C.M., and Hibbs, R.E. (2016). X-ray structure of the human α4β2 nicotinic receptor. Nature *538*: 411–415.

Moroni, M., Vijayan, R., Carbone, A., Zwart, R., Biggin, P.C., and Bermudez, I. (2008). Non-Agonist-Binding Subunit Interfaces Confer Distinct Functional Signatures to the Alternate Stoichiometries of the α4β2 Nicotinic Receptor: An α4–α4 Interface Is Required for Zn2+ Potentiation. J. Neurosci. *28*: 6884–6894.

Nielsen, B.E., Minguez, T., Bermudez, I., and Bouzat, C. (2018). Molecular function of the novel α7β2 nicotinic receptor. Cell. Mol. Life Sci. *75*: 2457–2471.

Oliveira, A.S.F., Shoemark, D.K., Campello, H.R., Wonnacott, S., Gallagher, T., Sessions, R.B., et al. (2019). Identification of the Initial Steps in Signal Transduction in the α4β2 Nicotinic Receptor: Insights from Equilibrium and Nonequilibrium Simulations. Structure *27*: 1171-1183.e3.

Purohit, P., and Auerbach, A. (2013). Loop C and the mechanism of acetylcholine receptor–channel gating. J Gen Physiol *141*: 467–478.

Puskar, N.L., Xiu, X., Lester, H.A., and Dougherty, D.A. (2011). Two Neuronal Nicotinic Acetylcholine Receptors, α4β4 and α7, Show Differential Agonist Binding Modes. J. Biol. Chem. *286*: 14618–14627.

Rego-Campello, H., Del Villar, S.G., Honraedt, A., Minguez, T., Oliveira, A.S.F., Ranaghan, K.E., et al. (2018). Unlocking Nicotinic Selectivity via Direct C–H Functionalization of (−)-Cytisine. Chem *4*: 1710–1725.

Revah, F., Bertrand, D., Galzi, J.-L., Devillers-Thiéry, A., Mulle, C., Hussy, N., et al. (1991). Mutations in the channel domain alter desensitization of a neuronal nicotinic receptor. Nature *353*: 846–849.

Sokalingam, S., Raghunathan, G., Soundrarajan, N., and Lee, S.-G. (2012). A Study on the Effect of Surface Lysine to Arginine Mutagenesis on Protein Stability and Structure Using Green Fluorescent Protein. PLOS ONE *7*: e40410.

Sousa da Silva, A.W., and Vranken, W.F. (2012). ACPYPE - AnteChamber PYthon Parser interfacE. BMC Research Notes *5*: 367.

Tonstad, S., Davies, S., Flammer, M., Russ, C., and Hughes, J. (2010). Psychiatric Adverse Events in Randomized, Double-Blind, Placebo-Controlled Clinical Trials of Varenicline. Drug-Safety *33*: 289–301.

Williams, D.K., Stokes, C., Horenstein, N.A., and Papke, R.L. (2009). Differential Regulation of Receptor Activation and Agonist Selectivity by Highly Conserved Tryptophans in the Nicotinic Acetylcholine Receptor Binding Site. J Pharmacol Exp Ther *330*: 40–53.

Zhang, J., Xue, F., Whiteaker, P., Li, C., Wu, W., Shen, B., et al. (2011). Desensitization of α7 Nicotinic Receptor Is Governed by Coupling Strength Relative to Gate Tightness. J. Biol. Chem. *286*: 25331–25340.

Figure Legends

Figure 1. A) Chemical structure of the agonists ACh, cytisine and 10-methylcytisine. **B)** Dynamical behavior of ACh, cytisine and 10-methylcytisine bound to one agonist site in the human $\alpha4\beta2$ and $\alpha7$ nAChR subtypes. Probability density maps (with a 0.00001 $Å^{-3}$ contour) for the positively charged group of the agonists are depicted as a blue mesh. The structure used as the starting point for the simulations is shown in grey. Abbreviations: cytisine, Cyt and 10-methylcytisine, MeCyt.

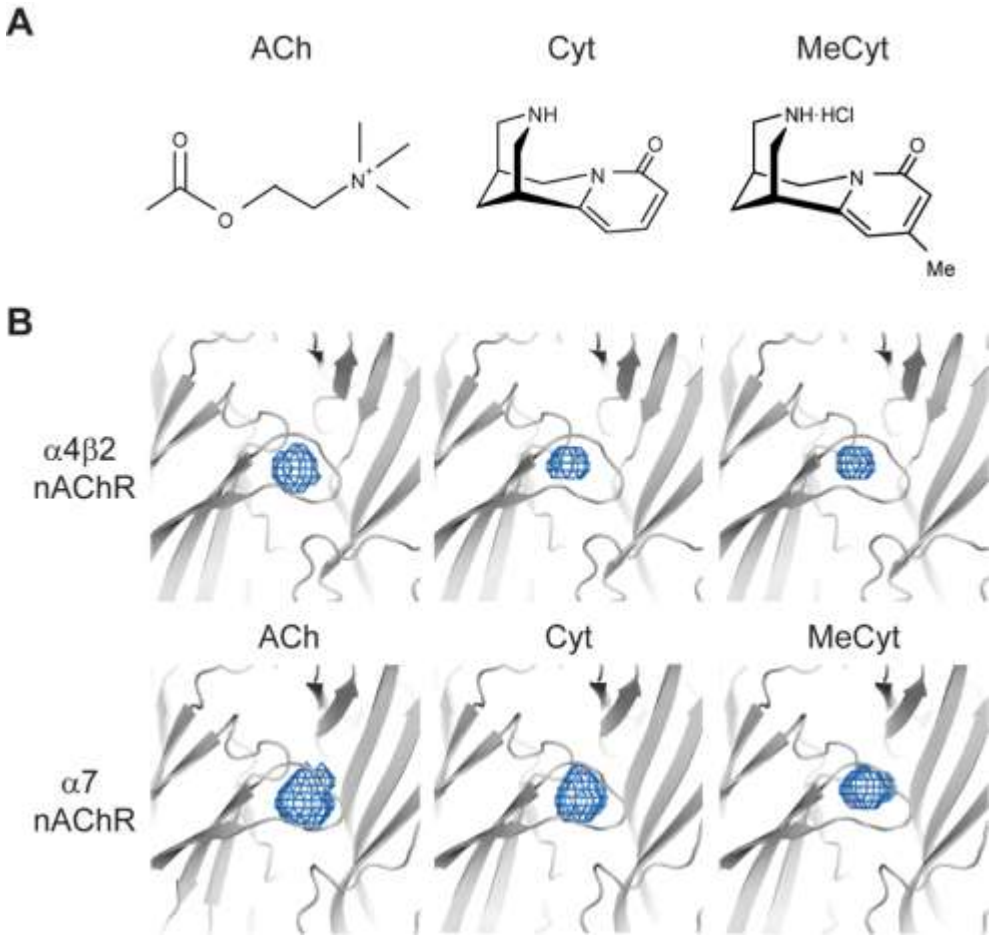

Figure 2. Dynamical behavior of the β3-strand arginine in **A)** α7 and **B)** α4β2 nAChR subtypes. Probability density maps for the arginine side chain are represented as a green mesh (contours at 0.00001 $Å^{-3}$ for the Cζ). In the α7 nAChR, R101 is highly mobile, whereas in the α4β2 the equivalent residue (β2R106) mobility is reduced due to an interaction with α4D185 in loop B. The principal and complementary subunits are coloured in blue and orange, respectively. 10-methylcytisine (MeCyt) is represented in grey with sticks and spheres. In the α7 nAChR, R101 moves close to the methyl group at the C(10) position. **C)** Time evolution of the distance between the positively charged group of 10-methylcytisine and the side chain of TyrC1 and TyrC2 in loop C in the α7 nAChR.

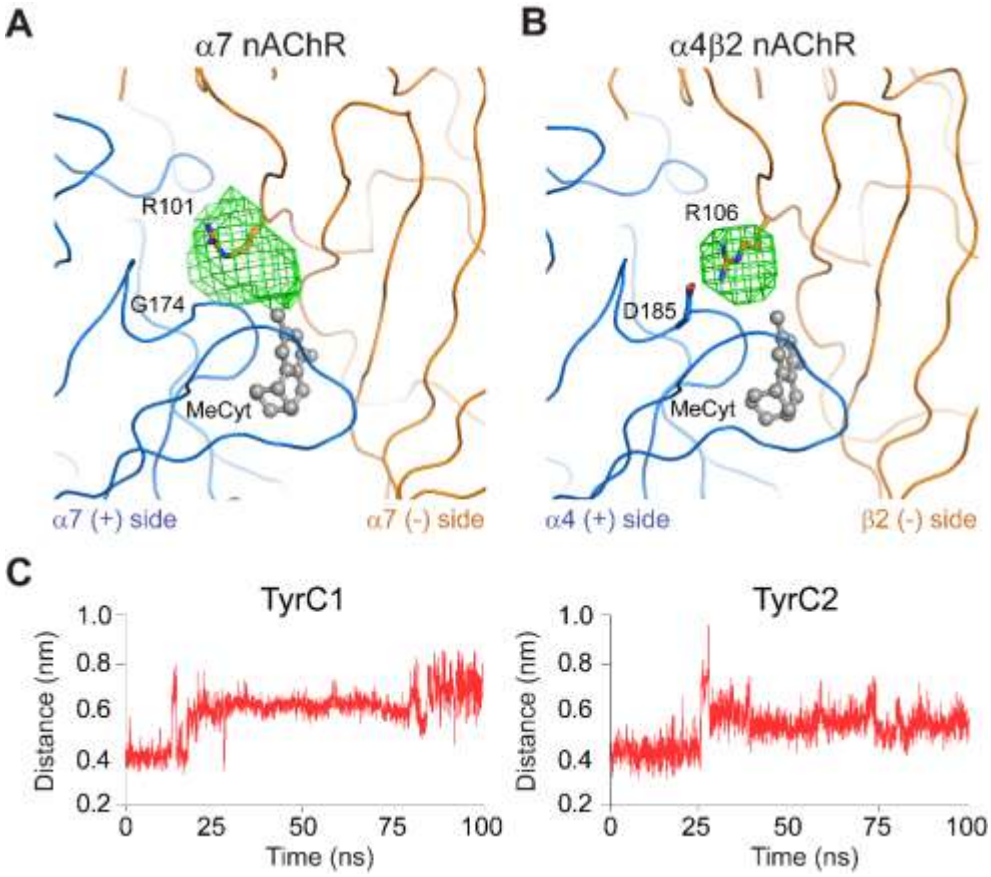

Figure 3. Overall distribution of the minimum distance between the sidechain of **A)** α7R101 and α7E215 in loop C and between β2R106 and **B)** α4D185 or **C)** α4E228. The histograms reflect the distances over the two nonconsecutive binding pockets of the receptors. Panels on the right show the position of the side chains of α7R101 and α7E215 and β2R106 and α4D185, α4D185 and α4E228 in the binding pockets. The principal subunit is shown in blue and the complementary in orange. The residues numbering refers to the following UniProt sequence codes: P43681 (α4 subunit), P17787 (β2 subunit) and P36544 (α7 subunit). Note that we include the signal peptide in the numbering. Abbreviations: cytisine, Cyt and 10-methylcytisine, MeCyt.

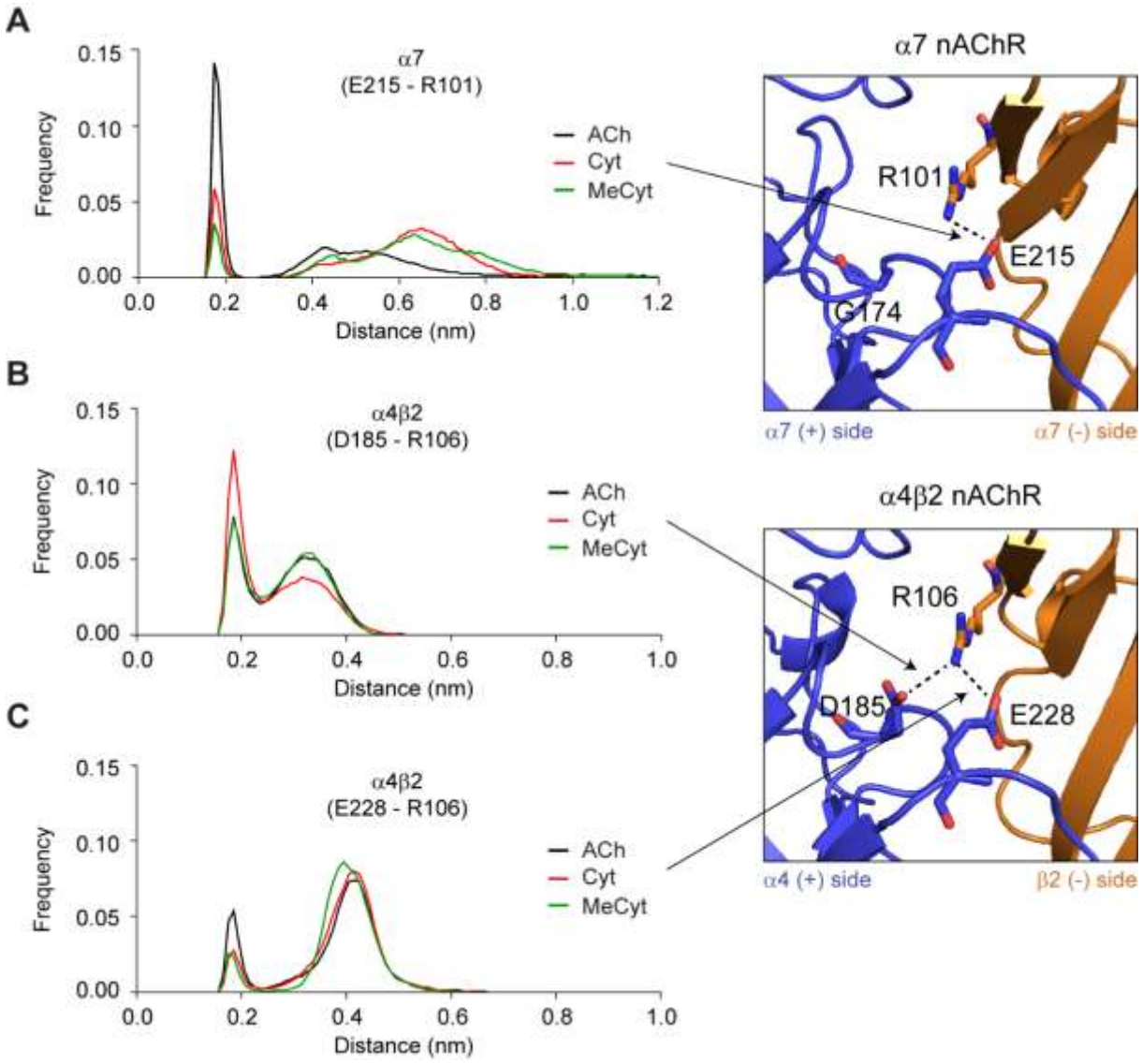

Figure 4. R101-D174 sal-bridge in MD simulations of α7G174D complexes. Overall distribution of the minimum distance between the sidechains of R101 (complementary subunit) and **A)** D174 (principal subunit) or **B)** E215 (principal subunit) in the α7G174D mutant receptor. The histograms reflect the distances over the two binding pockets bound to ACh (black line), cytisine (red line) and 10-methylcytisine (green line). Overall distribution of the distance between the charged N atom of cytisine and the sidechain of **C)** TyrA (α7115) or **D)** TrpD (α7W77), two main conserved aromatic residues lining the binding pockets in the α7 (black line) and α7G174D (orange line) systems. Panel on the right shows the position of D174, R101 and E215 in the cytisine-bound α7 complex. Abbreviations: cytisine, Cyt; 10-methylcytisine, MeCyt.

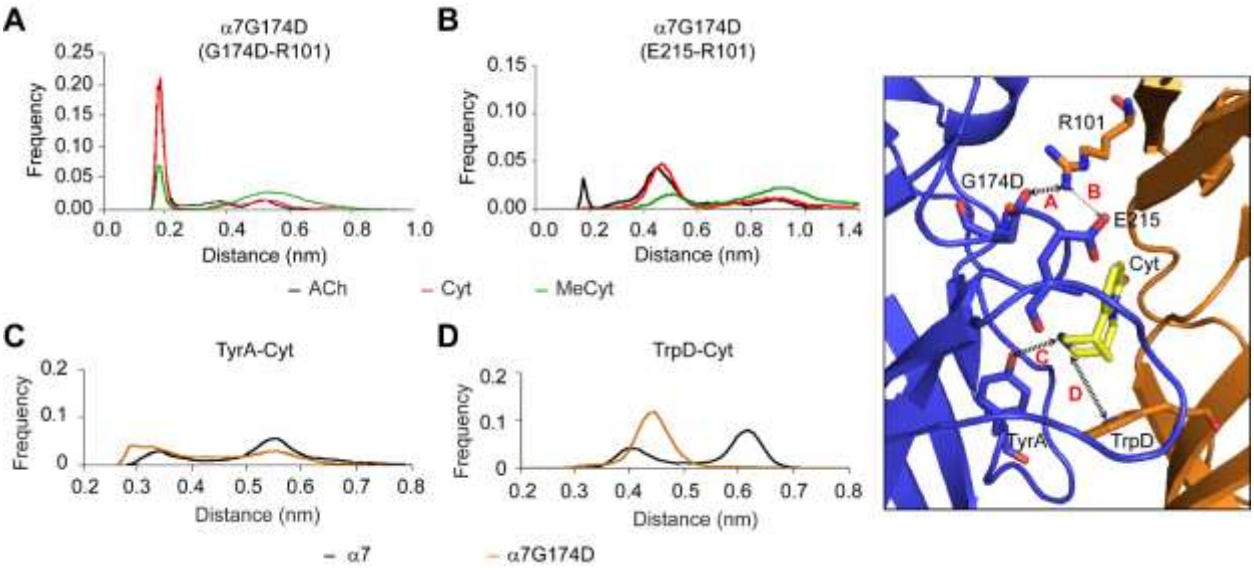

Figure 5. Functional effects of the R101-G174D salt-bridge. **A)** Agonist concentration-response curves for wild type α7 (black line and circles) and α7G174D (red line and squares) receptors. **B)** Distances between residues in positions 101 of β3-strand and 174 of loop B in α7 nAChRs. **C)** Functional effects of changes in distance between the charged moieties of residues at position 174 in loop B and 101 in β3 strand in wild type and mutant α7 nAChRs. The concentration-response curves shown are for ACh at α7 wild type (black circles and line) and mutant α7G174D,R101K (yellow diamonds and line) and α7G174E,R101K (purple triangles and line) nAChR. Data points in the concentration-response curves shown in A and C represent the mean ± SEM of 10-12 experiments carried out using 6-8 different *Xenopus* donors. Peak current amplitudes for all agonists were normalized to the maximal ACh response (1 mM). Estimated parameters EC_{50} and maximal relative efficacy (I_{Max}/I_{MaxACh}) are shown in Table 1. Abbreviations: cytisine, Cyt and 10-methylcytisine, MeCyt

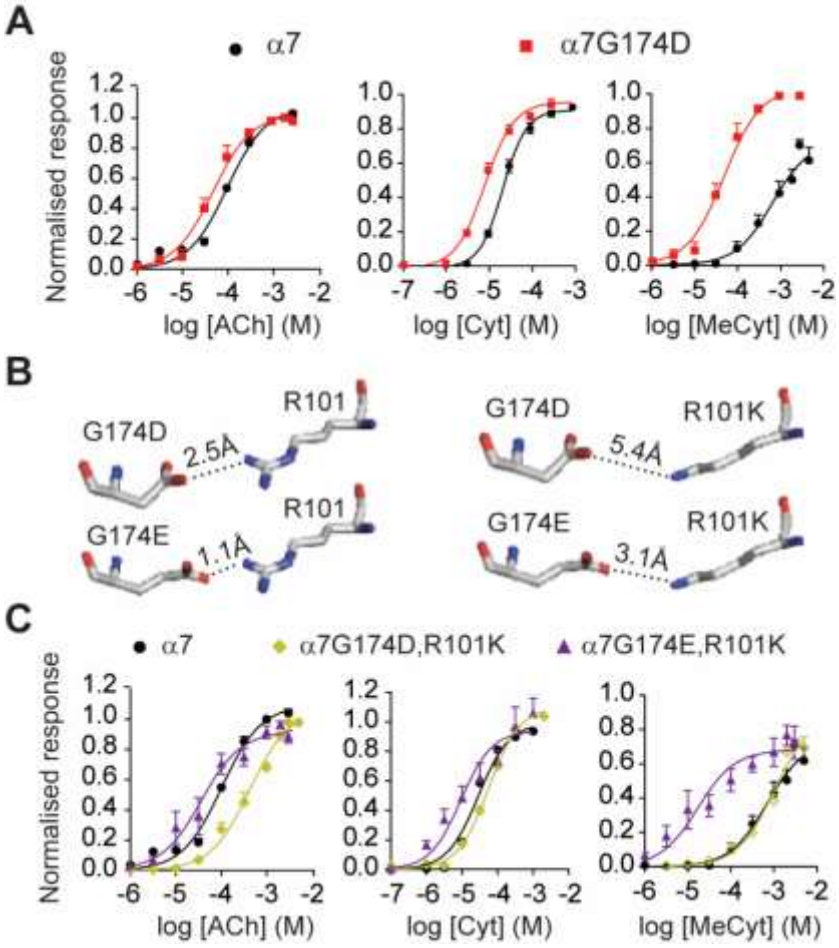

Figure 6. Comparison between single-channel profiles of α7 and α7G174D nAChR activated by ACh or cytisine. **A)** Typical traces of single-channel currents activated by ACh (top traces) or cytisine (bottom traces) in α7 and α7G174D receptors. Single-channel currents were measured using the cell-attached configuration on BOSC23 cells transiently expressing wild type α7 or α7G174D receptors. **B)** Bar chart of the mean open (τ_{open}, black) and burst (τ_{burst}, grey) durations for α7 and α7G174D in presence of ACh or cytisine at their EC_{50} concentrations. Data were obtained from single-channel recordings at a membrane potential of -70 mV. The open time corresponds to the longest component of the open time histogram. Burst durations were determined by the longest component of the burst histogram. **C)** Typical traces of macroscopic currents elicited by 1 mM ACh in α7 and α7G174D receptors expressed in *Xenopus* oocytes. The onset and overall decay of the currents in α7 and α7G174D are undistinguishable. Abbreviations: cytisine, Cyt and 10-methylcytisine, MeCyt.

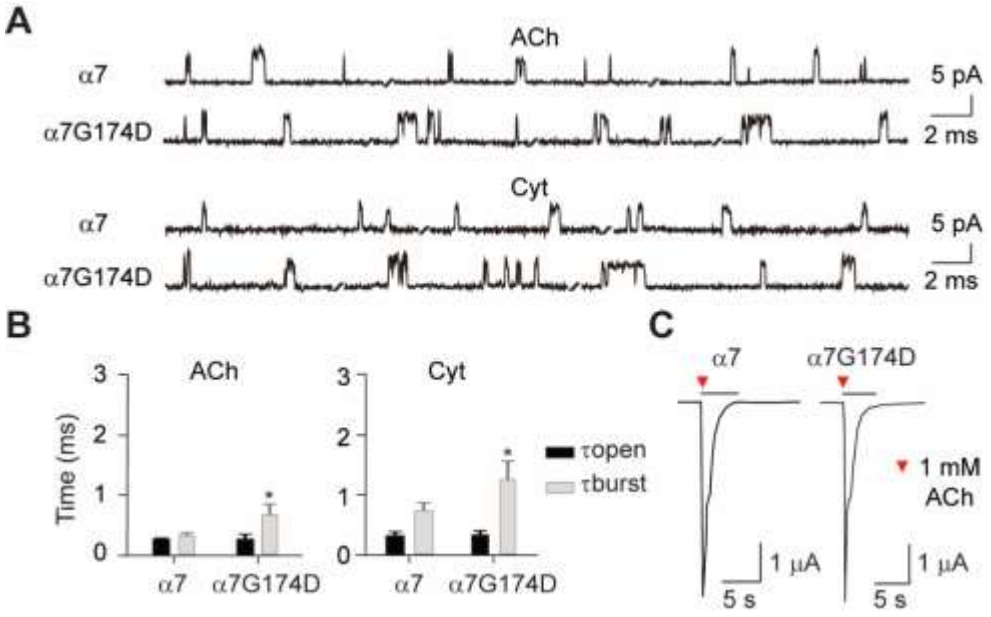

Figure 7. Macroscopic and microscopic current responses of α7R101A nAChR to agonists. **A)** Agonist concentration response curves for ACh, cytisine and 10-methylcytisine in wild type α7 (black line and circles) or α7R101A (blue line and triangles) receptors. Data points represent 10-12 experiments carried out in 6 to 8 different batches of *Xenopus* oocytes. **B)** Typical traces of the macroscopic current responses for ACh at wild type α7, α7R101A and α7R101D receptors. Note that the onset of decay and overall decay duration depends on the nature of residue in position 101 in the α7 nAChR. **C)** Single-channel currents activated in α7 or α7R101A nAChRs by EC_{50} ACh or EC_{50} cytisine. Recordings were made in the cell-attached patch configuration at a membrane potential of -70 mV, as detailed in SI. Abbreviations: cytisine, Cyt and 10-methylcytisine, MeCyt.

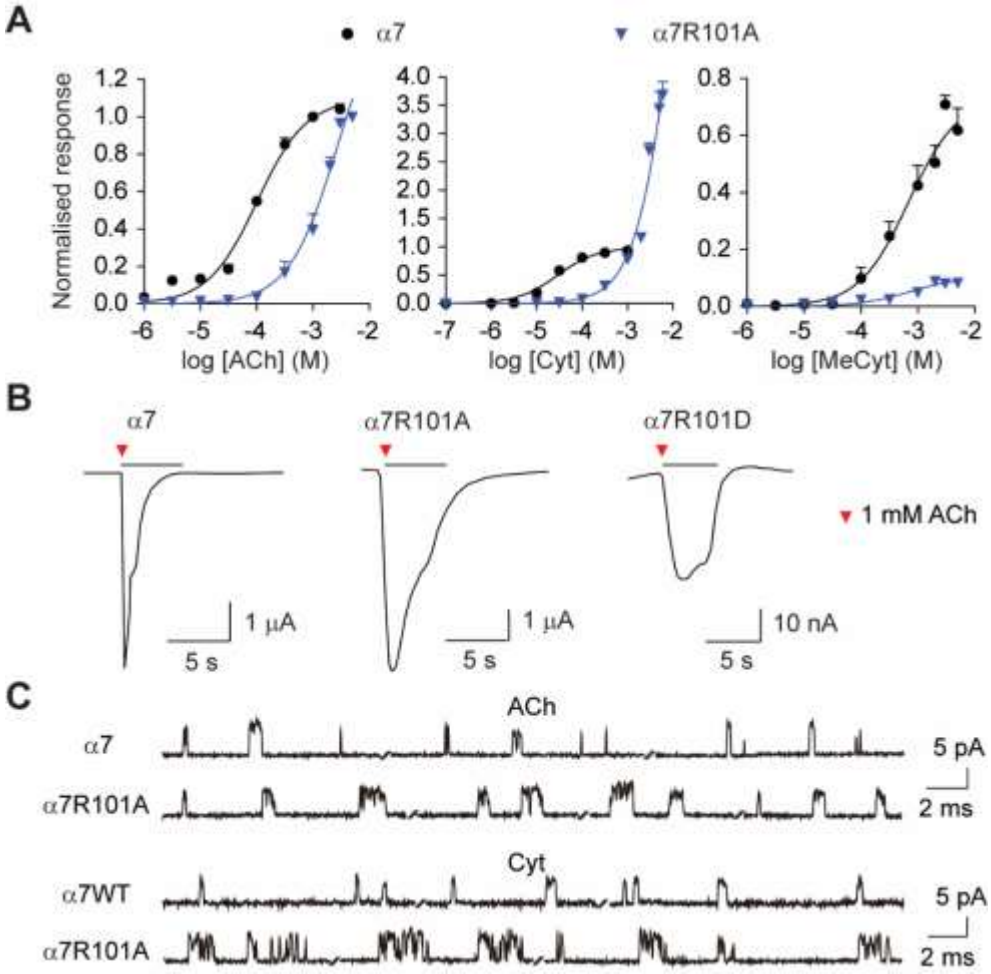

Figure 8. Average RMSF difference between α7 and α7R101A systems. **A)** Average change in Cα RMSF between the α7 and α7R101A systems with ACh (black line) cytisine (red line) or 10-methylcytisine (green line) bound in one of the two nonconsecutive binding pockets of the receptor. The RMSF differences for the principal (left side image) and complementary (right side image) subunits are shown. See SI Figure S8 to for the corresponding data obtained from the second binding pocket. **B)** Average RMSF difference between α7 and α7R101A systems bound to ACh, cytisine or 10-methylcytisine mapped into the average structure of each system. The structure colours are related to the average RMSF difference: the red and blue regions correspond to the residues with the largest differences between the two systems. Abbreviations: cytisine, Cyt and 10-methylcytisine, MeCyt.

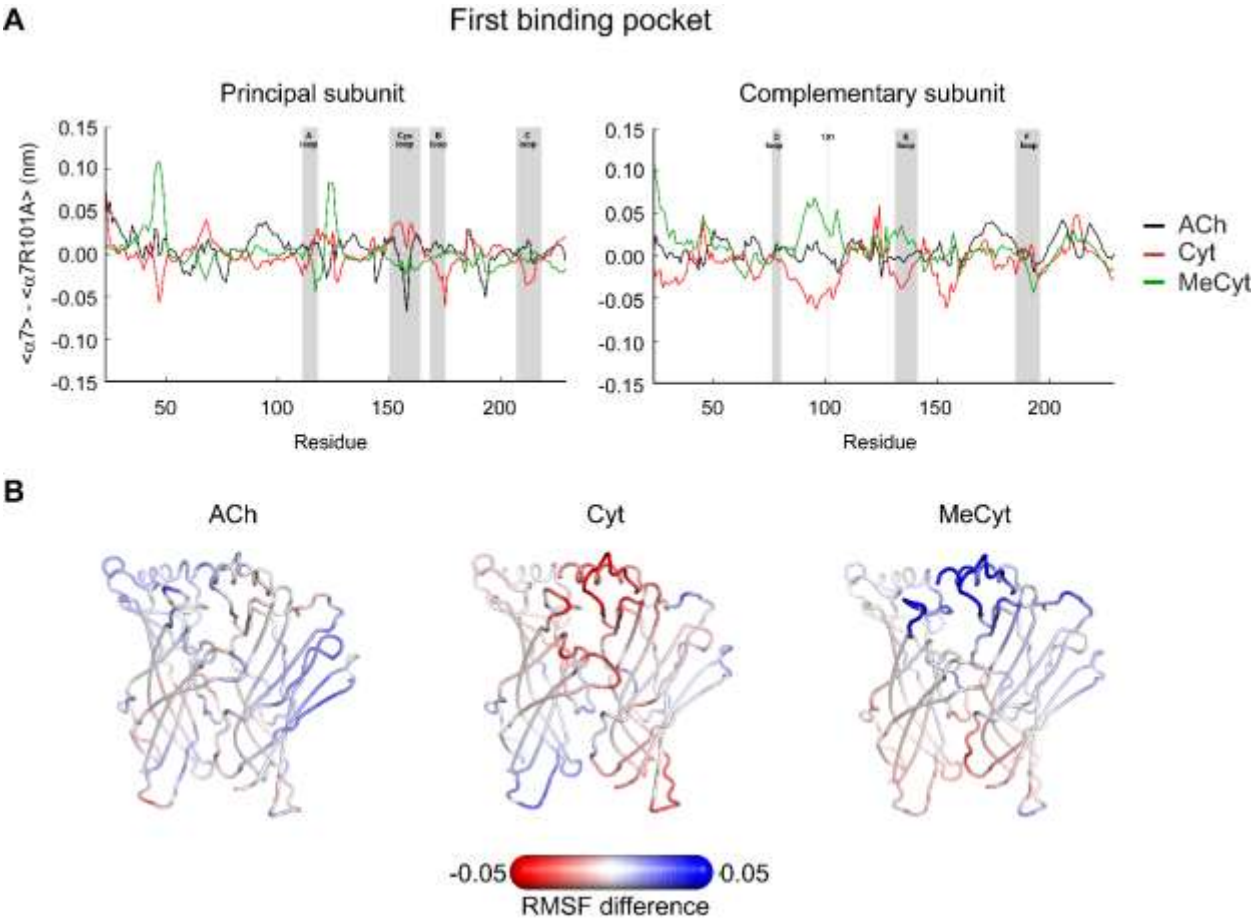

Figure 9. Average structure of agonist-bound α7 and α7R101A complexes. The agonist simulated were **A)** ACh, **B)** cytisine and **C)** 10-methylcytisine bound in one of the two nonconsecutive binding pockets of the receptor. Note that for the cytisine-bound α7R101A complex (shown in blue), there is a clear change in the extent of loop C capping, compared to α7 wild type (shown in gray) nAChR. The structures shown here represent the average structure calculated over all replicates for each system, as described in Materials and Methods. Abbreviations: cytisine, Cyt and 10-methylcytisine, MeCyt.

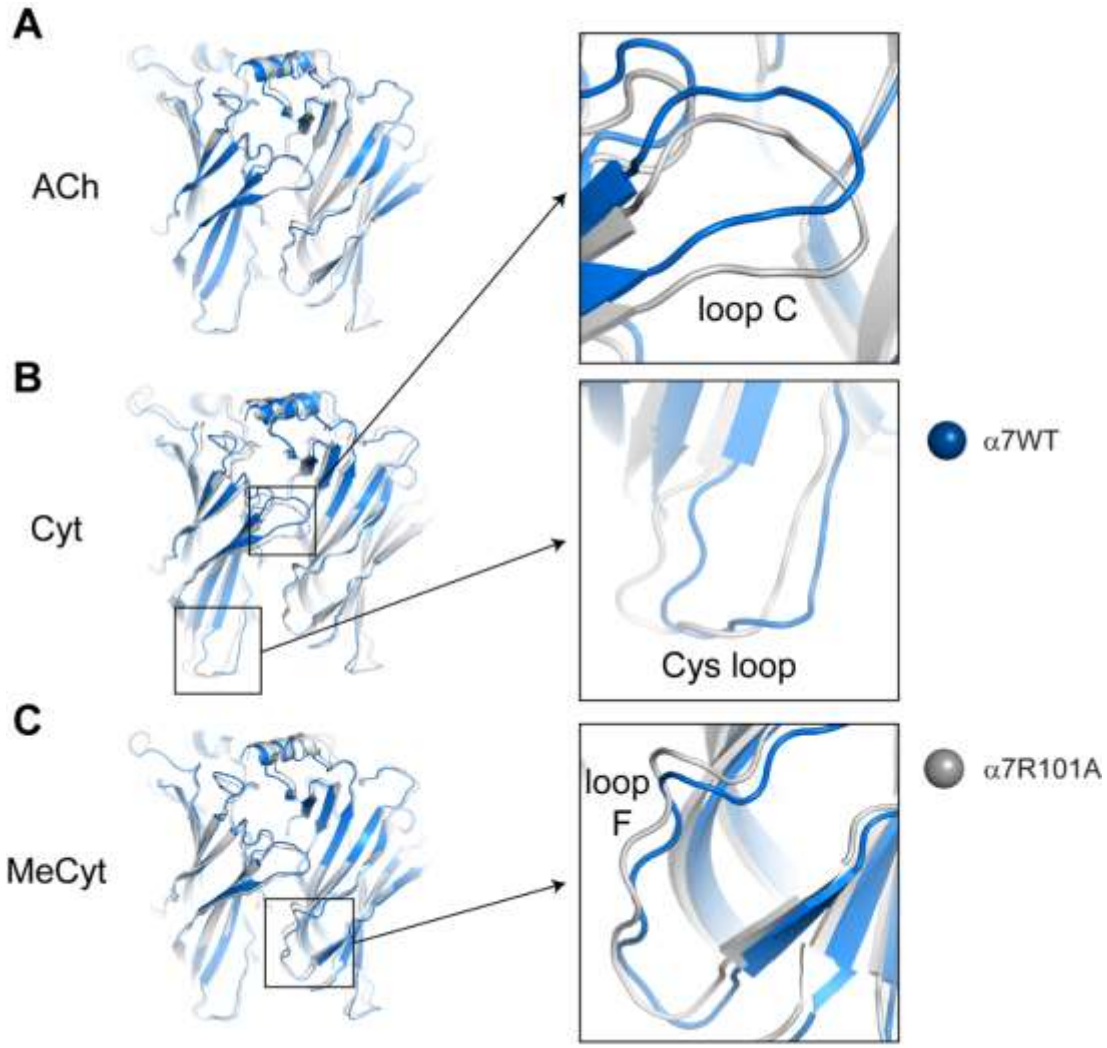

Table 1. R101 of β3-strand influence agonist potency and efficacy in the α7 nAChR subtype.

	ACh		Cytisine		10-Methylcytisine	
Mutation	**EC_{50} (μM) (95% CI)**	**I_{max}/I_{AChMax} (95% CI)**	**EC_{50} (μM) (95% CI)**	**I_{max}/I_{AChMax} (95% CI)**	**EC_{50} (μM) (95% CI)**	**I_{max}/I_{AChMax} (95% CI)**
α7	82.4 (71-95)	1	29.64 (24-37)	0.93 (0.90-0.94)	643 (493-837)	0.55 (0.4-0.7)
α7G174D	66.9 (37-120)	1	8.5* (5.4-7.4)	0.95 (0.8-1.1)	139.6*** (100-190)	0.92** (0.8-1.0)
α7G174A	86 (38-194)	1	60.11 (19-191)	1.40 (1.0-1.8)	891 (545-1459)	0.40 (0.2-0.6)
α7G174E	322 ** (181-568)	1	272.9*** (161-463)	1.17 (0.8-1.5)	1025.6*** (120-8749)	0.75 (0.5-0.9)
α7R101A	887.2*** (565-1393)	1	389*** (299-504)	4.10*** (2.4-6.0)	2075*** 440-7943	0.39 (0.06-0.85)
α7R101D	ND	1	ND		ND	
α7R101D, G174R	ND	1	ND		ND	
α7R101K	741.3*** (506-1086)	1	121.6** (63-236)	1.05 (0.8-1.3)	3228* (2523-4130)	0.56 (0.2-0.9)
α7G174D, R101K	349.1*** (222-550)	1	54 (25-112)	1.26 (1.1-1.5)	1303.2 (902-1888)	0.96* (0.7-1.2)
α7G174E, R101K	54 (36-79)	1	7.81* (3-20)	1.04 (0.8-1.3)	69.34*** (36-132)	0.68 (0.5-0.8)
α7E215A	148* (83-260)	1	85.9* (52-140)	1.12 (1.0-1.3)	1140* (756-1713)	0.95 (0.6-1.2)

EC_{50} and normalised maximal current responses (relative efficacy) (I_{Max}/I_{AChMax}) were estimated as described in Methods**.** Data shown represent the mean +/- 95% confidence interval (CI) of n= 10-12 experiments carried out in 6 to 8 different batches of *Xenopus* oocytes. Statistical differences between α7WT and α7 mutant receptors were determined by One Way Anova followed by Dunnett's or Bonbeforri's post-tests. Levels of statistical significance: *p < 0.05; ** p < 0.01; *** p < 0.001. ND, not determined due to low levels of functional expressions (less than 100 nA of ACh maximal currents).

Table 2. Microscopic currents of wild type and mutant α7 nAChR receptors.

Agonist	Receptor	τ_{open} (ms)	τ_{burst} (ms)	n	N
ACh	α7	0.27 ± 0.02	0.33 ± 0.06	6	5
	α7G174D	0.26 ± 0.10	0.69** ± 0.17	5	5
	α7R101A	0.29 ± 0.04	1.41*** ± 0.41	5	5
Cytisine	α7	0.28 ± 0.09	0.72 ± 0.12	6	5
	α7G174D	0.31 ± 0.08	1.25* ± 0.30	4	5
	α7R101A	0.29 ± 0.10	2.00*** ± 0.26	7	5

τ_{open} and τ_{burst} correspond to the longest components of the corresponding open time and burst duration histograms. Values are mean ± SD. n: number of independent experiments, each from different cell patches. N: number of cell transfections. Statistical significance was determined by comparing the mean value in the mutant receptor respect to the mean value in the wild type α7 receptor for each agonist, by two-tailed Student's t-test ($p<0.05$*, $p<0.01$**, $p<0.001$***). N corresponds to number of transfected cell batches used and n is the number of recordings carried out.